Research Article

Ivan G. Kazantsev*, Rauan Z. Turebekov and Murat A. Sultanov

Inpainting of regular textures using ridge functions

https://doi.org/10.1515/jiip-2021-0053
Received July 30, 2021; revised December 28, 2021; accepted January 5, 2022

Abstract: In this paper, we propose a method for inpainting regular textures composed of oriented patterns and completion of images distorted by long stripes. We have developed a model fit to describe a regular texture as a sum of a few ridge functions. The ridge functions are known in tomography as a result of a back-projection operator applied to projections, or samples of the Radon transform. A computational scheme for the singular value decomposition of a regular texture into the sum of informative ridge functions is presented. The numerical experiments on various images demonstrate the efficiency of the techniques proposed.

Keywords: Radon transform, ridge function, image inpainting, texture

MSC 2010: 44A12, 68U10

1 Introduction

Textures as well as contours and salient points are important objects in the image analysis and computer vision tasks. To date, many methods have been developed for the quantitative description of textures, and they continue to develop. Since images have a tremendous variety, various approaches [15] from such fields of knowledge as applied mathematics, optics, biology, statistics, signal theory, integral geometry, etc., are used to represent textures. Textures are conventionally divided [4] into two large classes: stochastic and regular. Stochastic textures are observed in the nature around us, while regular textures appear more often as a result of human activity. In a more comprehensive categorisation, four different approaches to the texture analysis [18] can be distinguished: statistical, geometric, model-based and signal processing approaches. For all types of textures, it would be desirable if one could derive their mathematical description aimed at the computer-aided modeling in such areas as pattern classification [8], texture modelling [12, 19], industrial design [20], detection of fabric defects [3, 11, 14], etc.

In this paper, we deal with a model-based class of regular and near-regular textures that can be represented as a sum of ridge functions using the Radon transform and its singular value decomposition [13]. We provide a constructive approach to fitting such a model to a given texture. Ridge functions [5–7, 10, 16] and their directions are used as the main descriptors of linear structures, their combinations and oriented textures. Some of them such as a linear part of roads and buildings in an aerial image are treated as a single ridge function. Other ones, such as regular textures in fabrics, are perceived as the sum of a few ridge functions. Some imperfections are locally regular objects (scratches and wrinkles in photos, rain drops on camera optics, etc.), and others, on the contrary, are a lack, or disorder of regularity against the background of a certain pattern. Impressive results obtained with classical methods of partial differential equations applied in

***Corresponding author: Ivan G. Kazantsev,** Institute of Computational Mathematics and Mathematical Geophysics, Novosibirsk 630090, Russia, e-mail: kazantsev.ivan6@gmail.com. https://orcid.org/0000-0002-8479-7349
Rauan Z. Turebekov, Murat A. Sultanov, Khoja Akhmet Yassawi International Kazakh–Turkish University, Turkestan 161200, Kazakhstan, e-mail: rauan.turebekov@ayu.edu.kz, murat.sultanov@ayu.edu.kz

the new field of "inpainting" [1, 9, 17] motivate us to explore the ridge functions and their orientation as indicators to the recovery or the removal of repetitive structures in an image.

The paper structure is as follows. In Section 2, we revisit the methods relevant to the image reconstruction using the ridge functions. Section 3 outlines a concept of projection information content. In Section 4, we present a scheme for the background and regular texture separation. In Section 5, we show the results of numerical experiments with the texture decomposition and inpainting in test images. In Section 6, we illustrate the results of detecting the local defect in a real-world textile sample. We present our conclusion in Section 7.

2 The Radon transform and ridge functions

We interpret the functions f as images with a support in the form of the unit disk D.

Definition 2.1. The Radon transform R of the function f is defined as the set of its integrals along a line with direction α and distance s from the origin

$$R_\alpha[f](s) = \int_{-\sqrt{1-s^2}}^{\sqrt{1-s^2}} f(s\cos\alpha - t\sin\alpha, s\sin\alpha + t\cos\alpha)\,dt. \tag{2.1}$$

We denote a single projection (2.1) as $p(\alpha, s) = p_\alpha(s)$ and refer to it as a complete projection if it is known for all points in the interval $s \in [-1, 1]$. In practical tomographic reconstructions, only a limited number of projections and a finite number of samples per projection are available. Let us recall the definition of the ridge functions [5, 10, 16].

Definition 2.2. A ridge function $h(x, y)$ on D is understood as a function of the form

$$h(x, y) = h(x\cos\alpha + y\sin\alpha).$$

If a set of directions of the projections is the n-tuple $\omega = (\omega_1, \ldots, \omega_n) \in [0, \pi)^n$, then we denote the corresponding set of complete projections by

$$R_\omega[f] = (R_{\omega_1}[f], \ldots, R_{\omega_n}[f]).$$

Tomographic scanners, recording a sufficient number of projections with equally distributed direction angles, provide the reconstruction of the function f from the data R_ω in the form of the filtered back-projection (FBP) approximation that reads as

$$f(x, y) \approx \sum_{i=1}^{n} r_i(x\cos\omega_i + y\sin\omega_i). \tag{2.2}$$

Here, the function r_i is defined as $r_i(s) = \int_{-\infty}^{\infty} p(\omega_i, t)k(s - t)\,dt$. For each r_i the same kernel k is used [13]. Formula (2.2) expresses the approximation of the function f as superposition of the ridge functions r_i with the directions ω_i uniformly distributed in the interval $[0, \pi)$. However, in the case of an arbitrary set of the directions $\omega = (\omega_1, \ldots, \omega_n) \in [0, \pi)^n$, different convolution kernels k have to be used for different directions. It is known that generally the FBP approximation is not accurate in the case of a small ($n < 10$) number of projections.

The alternative approach providing a better accuracy in case of small n is based on the following approach by Logan and Shepp [10]. The representation they use is similar to (2.2)

$$H(x, y) = \sum_{i=1}^{n} h_{\omega_i}(x\cos\omega_i + y\sin\omega_i), \tag{2.3}$$

which satisfies the Radon transform-based constraints

$$R_{\omega_i}[f] = R_{\omega_i}[H], \quad i = 1, \ldots, n. \tag{2.4}$$

The minimum norm solution to problem (2.3)–(2.4) has the following form:

$$h_{\omega_i}(s) = \frac{1}{\pi} \sum_{k=1}^{\infty} \sum_{j=1}^{n} \eta_{ij}^{(k)} U_{k-1}(s) \int_{-1}^{1} p_{\omega_j}(t) U_{k-1}(t)\, dt, \tag{2.5}$$

where $p_{\omega_j}(t) = R_{\omega_j}[f](t)$, $U_{k-1}(t) = \frac{\sin(k \arccos t)}{\sin(\arccos t)}$, $k = 1, 2, \ldots$, are the Chebyshev polynomials of the second kind, $\eta_{ij}^{(k)}$ are entries of the matrix Λ_k^+ (generalized inverse), $\Lambda_k = (\lambda_{ij}^{(k)})$, $i, j = 1, \ldots, n$, $\lambda_{ij}^{(k)} = \frac{\sin(k(\omega_i - \omega_j))}{k \sin(\omega_i - \omega_j)}$.

Equation (2.5) provides us with the singular value decomposition (SVD) solution of the Radon transform inversion task. It can be shown that the norm of H can be calculated using the projections $p_i \equiv p_{\omega_i}$

$$\|H\|^2 = \frac{1}{\pi} \sum_{k=1}^{\infty} \sum_{i,j=1}^{n} \eta_{ij}^{(k)} \int_{-1}^{1} p_{\omega_i}(s) U_{k-1}(s)\, ds \int_{-1}^{1} p_{\omega_j}(t) U_{k-1}(t)\, dt. \tag{2.6}$$

The directions ω can be arbitrary, and for the generalized pseudo-inversion of the matrices Λ_k we use the *pinv* function of the Matlab package. The integrals $\int p_{\omega_j}(t) U_{k-1}(t)\, dt$ in formulas (2.5) and (2.6) can be calculated using the Gauss–Chebyshev quadrature formula

$$\int_{-1}^{1} \frac{g(t)}{\sqrt{1-t^2}}\, dt \cong \frac{\pi}{m} \sum_{l=1}^{m} g(t_l),$$

where $t_l = \cos(\frac{2l-1}{2m}\pi)$, $l = 1, \ldots, m$, are sampling points of a function g. Then formula (2.5) becomes

$$h_{\omega_i}(s) = \frac{1}{m} \sum_{k=1}^{\infty} \sum_{j=1}^{n} \eta_{ij}^{(k)} U_{k-1}(s) \sum_{l=1}^{m} p_j(t_l) \sin\Big(k \frac{2l-1}{2m}\pi\Big). \tag{2.7}$$

The truncation parameter m in series (2.7) is used for regularization of the SVD decomposition.

3 The information content of projections

We will extensively use a constructive algorithm (2.5) for computing the superposition of the ridge functions H_ω from an arbitrary set of complete projections R_ω. It is known that for a minimum norm solution H_ω, the following identity is valid:

$$\|f - H_\omega\|^2 = \|f\|^2 - \|H_\omega\|^2. \tag{3.1}$$

It follows from (3.1) that the knowledge of the norm $\|H_\omega\|^2$ is useful in estimating the accuracy of reconstruction (2.5) for an arbitrary set of projections. We consider n projections $R_\omega f = (p_{\omega_1}, \ldots, p_{\omega_n})$ of a given digital image f as its representatives, or features in computer vision tasks. Varying the vector ω, we can calculate the best SVD-approximation of the function f by a sum of the corresponding ridge functions $H_\omega = \sum_{j=1}^{n} h_{\omega_j}$. An interesting property of this representation is that a minimum norm solution is unique, but it is not a set of ridge functions generating the solution.

Definition 3.1. We refer to the quantity $Q(f, \omega) \equiv \|H_\omega(x, y)\|^2$ as information content, or the informativity of the projection set $R_\omega f$.

We say that the projection set $R_\omega f$ is more informative than the set $R_\alpha f$ if the inequality $Q(f, \omega) > Q(f, \alpha)$ holds. Given an image f and a number n, we can find the most informative set of the directions ω^* by a global search

$$\omega^* = \arg\max_{\omega} Q(f, \omega). \tag{3.2}$$

The projection data $R_{\omega_0}[f]$ obtained after the global search maximally stores the information about n elongated structures present in the image. It is easy to show that the information content of a single projection p_{ω_j} is

$$Q^S(f, \omega_j) \equiv \frac{1}{2} \int_{-1}^{1} (1 - s^2)^{-\frac{1}{2}} p_{\omega_j}^2(s)\, ds. \tag{3.3}$$

4 An image model with background and texture

Let us consider an additive model of image formation (distortion) in the form of the equation

$$z(x, y) = u(x, y) + v(x, y), \tag{4.1}$$

where z is the observed image, u is the desired useful image, as a rule, with many details, and v is a certain interfering structure, which is known to be well approximated by the sum of a small number of the ridge functions in n directions $\omega = (\omega_1, \dots, \omega_n)$. The task is to restore u from the data of z. Due to the additivity of model (4.1) and the linearity of the Radon transform, the expansion of the functions z, u, v into the superposition of the ridge functions in the directions ω results in the equality

$$Z_\omega = U_\omega + V_\omega. \tag{4.2}$$

Here, Z_ω, U_ω, V_ω are the minimum norm solutions obtained, respectively, by reconstructing the images z, u, v from the data sets $R_\omega[z]$, $R_\omega[u]$, $R_\omega[v]$.

Since it is known that the texture v is well approximated by the ridge functions in the directions ω, we have $v \approx V_\omega$. Then subtracting equation (4.1) from (4.2), we approximately obtain

$$z(x, y) - Z_\omega(x, y) = u(x, y) - U_\omega(x, y). \tag{4.3}$$

We hypothesize that the difference $u(x, y) - U_\omega(x, y)$ on the right-hand side of (4.3) is approximately similar to u with a shifted average value. Converting the image $z(x, y) - Z_\omega(x, y)$ to the range of values of a visualizing device, we synthesize an image to be essentially free from distortions caused by the presence of the texture v.

In the problem of detecting a defect in a textile image, the terms in equation (4.1) are as follows. The observed image is z, u is the anomaly, and v is the ideal texture of the fabric. The purpose of the detection is to separate u and v and then to test the hypothesis that there is a significant discontinuity u in the texture regularity.

5 The numerical experiments with texture inpainting

In our computer experiments, we use well-known (publicly available) test images "Cameraman" (Figure 1 (e) and Figure 2 (the upper row (a)), "Moon" (Figure 2, the bottom row (a)), "Pepper" and "Lake" (Figure 3 (the upper and bottom rows (a), respectively)) as the background images.

They are denoted as u and treated as useful images that are superimposed by the regular texture v, and the image $z = u + v$ is image (4.1) observed by the vision system. The textures v used are of the two types. The first one is the texture D52 "Oriental ornament" shown in Figure 1 (a), available from the album of textures by Brodatz [2]. In this case, informative directions are not known in advance and we need to investigate informative components of the texture numerically. The second type ot textures can be seen in Figure 2 and Figure 3, where we extensively use a regular texture generated as a sum of four ridge functions, in the form of a beam of parallel lines resembling dark and light scratches. In this case we construct parallel beams of scratches and therefore we know their orientations. Images in Figure 1 are of 128×128 size. Images in Figure 2 are of 256×256 size and the images "Pepper" and "Lake" in Figure 3 are of 512×512 size.

5.1 The first experiment

In the first experiment, we have numerically generated 180 projections of the texture D52, or the image v, with the directions $(0^\circ, 1^\circ, \dots, 179^\circ)$ and with 128 samples per projection that occupy columns of the sinogram space (Figure 1 (b)). We have calculated the values of the information content of individual projections using formula (3.3), and these values are presented in Figure 1 (c). For the texture D52, four informative directions turned out to be $\omega = (0^\circ, 48^\circ, 90^\circ, 131^\circ)$. The corresponding normal solution V_ω is shown in Figure 1 (d). As the background image u we use the test image "Cameraman" (Figure 1 (e)) and simulate its distortion as the

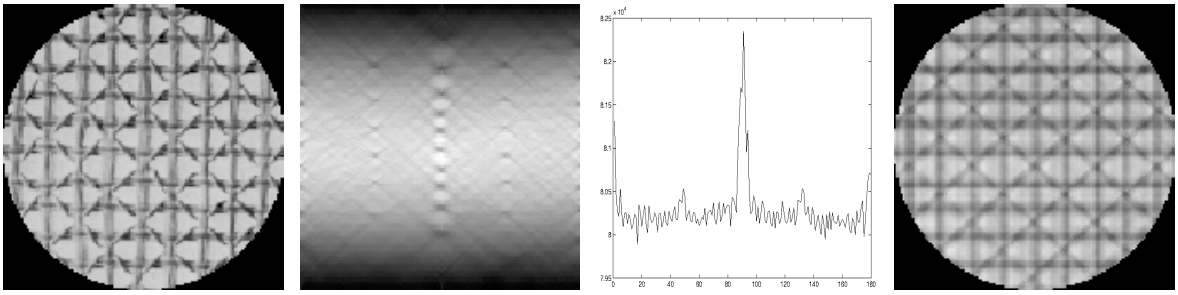

(a) (b) (c) (d)

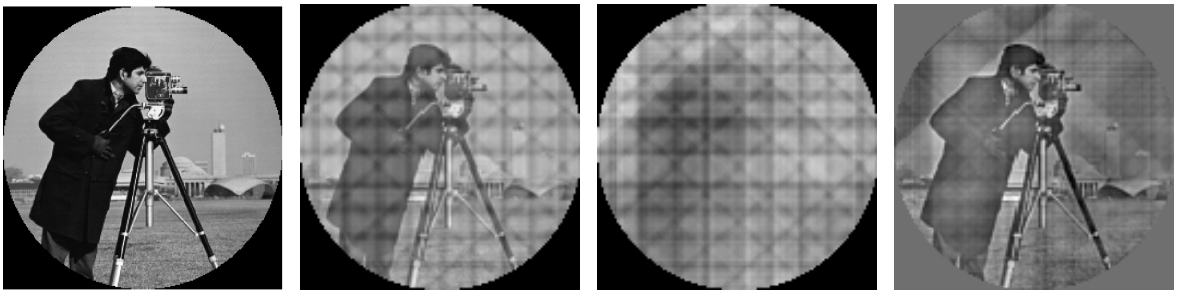

(e) (f) (g) (h)

Figure 1: (The upper row) (a) The texture image v, $\|v\|^2 = 85473$; (b) The Radon transform, or a sinogram of the image v; (c) The informativity Q^S of 180 projections; (d) Reconstruction V_ω of v from projections in the directions $\omega = (0°, 48°, 90°, 131°)$, $\|V_\omega\|^2 = 83757$, $\|V_\omega\|^2/\|v\|^2 = 0.98$; (e) The test image u; (f) The image $z = u + v$; (g) The ridge approximation Z_ω of z; (h) The difference $z - Z_\omega \approx u$.

sum $z = u + v$ (Figure 1 (f)). The SVD reconstruction Z_ω of z using the informative projections R_ω is shown in Figure 1 (g). The image of the difference $z - Z_\omega$ shown in Figure 1 (h) is improved in comparison with the image (f).

5.2 The second experiment

In Figure 2 (the upper and bottom rows), we show the experiments on the test background image u (the upper and bottom (a)), with the added texture v, numerically simulating four beams of a few parallel scratches (the upper and bottom (b)) in the directions $\omega = (17°, 37°, 107°, 127°)$. The SVD reconstruction Z_ω of u, given $z = u + v$, using the known informative projections R_ω is shown in Figure 2 (the upper and bottom (c)). The images of the difference $z - Z_\omega$ shown in Figure 2 (the upper and bottom (d)) are essentially improved in comparison with the images (b) (the upper and bottom rows, respectively). The scratches are generated so that some of them are randomly darker and others are brighter than the background useful image. Their location within the ridge function is unknown. We synthesize textures as a sum of a few ridge functions consisting of several narrow (of 1–2 pixels width) strips.

In Figure 3 (the upper and bottom rows) we repeat computations with a similar methodology of numerical experiments. The texture of 512×512 size numerically simulates a beam of many parallel scratches in the four known directions $\omega = (30°, 45°, 120°, 135°)$.

6 The textile defect extraction: A real-world example

To illustrate the task of computing the informative SVD reconstruction for the real-world problem of detecting defects in a textile image, we use a sample *a2R1.jpg* of a textile from the open dataset GLSR [21] (Figure 4 (a)).

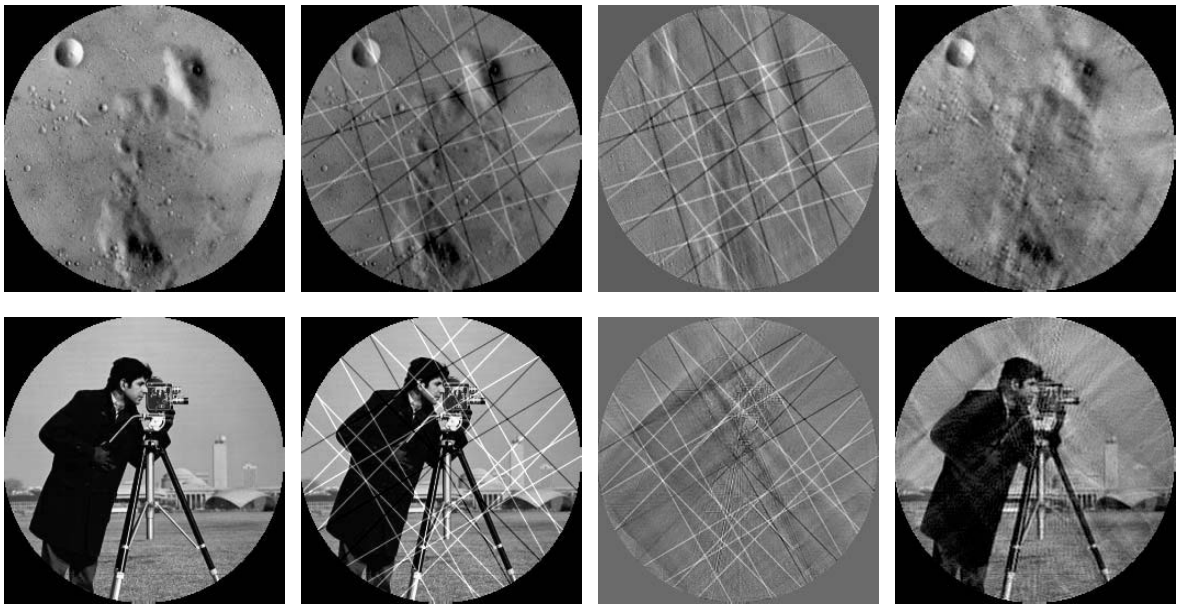

(a) (b) (c) (d)

Figure 2: (The upper and bottom rows) (a) The test image u; (b) The sum $z = u + v$ of the image u and the texture v represented by four sets of parallel lines in the directions $\omega = (17^\circ, 37^\circ, 107^\circ, 127^\circ)$; (c) The result of the SVD-based representation of z in the directions ω; (d) The difference $z - Z_\omega$ of images (b) and (c).

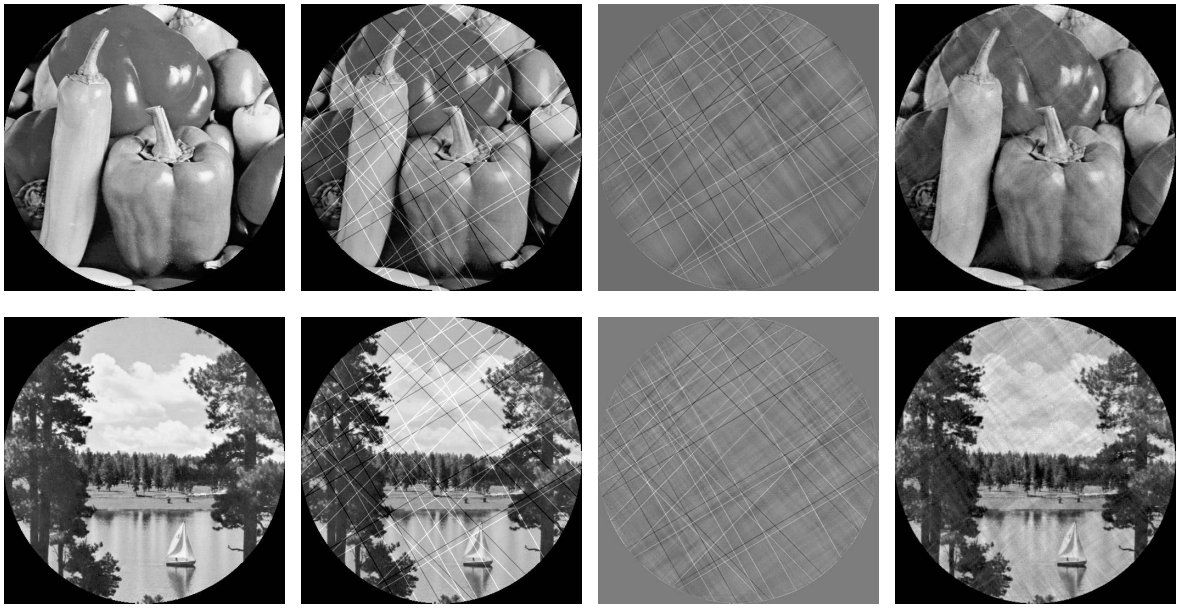

(a) (b) (c) (d)

Figure 3: (The upper and bottom rows) (a) The test image u; (b) The sum $z = u + v$ of the image u and the texture v represented by four sets of parallel lines in the directions $\omega = (30^\circ, 45^\circ, 120^\circ, 135^\circ)$; (c) The result of the SVD-based approximation Z_ω of z in the directions ω; (d) The difference $z - Z_\omega$ of images (b) and (c).

The textile is denoted as image z and it is supposed to contain a single defect u and a background texture v, and $z = u + v$. The texture z is limited to a circular domain within $n \times n$ image, $n = 256$. For the image z, n projections are numerically generated, evenly distributed in the range $[0, \pi)$, that is, with a discreteness of $180^\circ/n$. Each projection has $n = 256$ samples, so the Radon transform, or a sinogram, is the $n \times n$ image. The projections are arranged line by line in succession from top to bottom, counts ("detectors") make up the

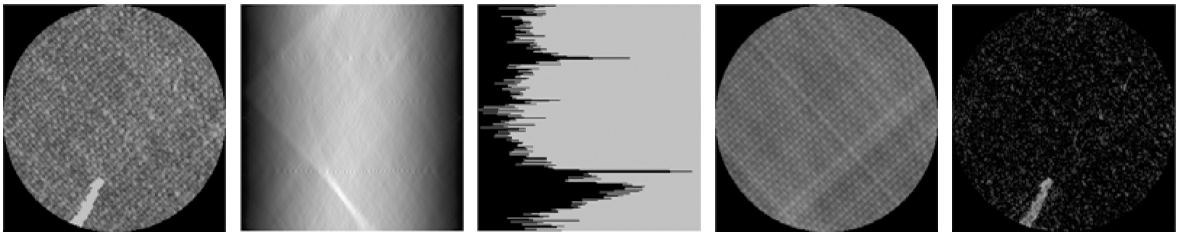

(a) (b) (c) (d) (e)

Figure 4: The textile sample *A2R1.jpg*. (a) The textile image z, $\|z\|^2 = 60831$; (b) The sinogram of z; (c) A plot of informativity Q^S; (d) Reconstruction Z_α from four projections in the directions $\alpha = (8^\circ, 42^\circ, 77^\circ, 132^\circ)$, $\|Z_\alpha\|^2 = 58653$, $\|Z_\alpha\|^2/\|z\|^2 = 0.96$; (e) The difference $z - Z_\alpha$ of images (a) and (d).

horizontal axis (Figure 4 (b)). The informativity values Q^S of individual n projections are calculated by formula (3.3), and then, by examining the local maxima, M projections in the directions $\alpha = (\alpha_1, \ldots, \alpha_M)$ are selected, from which the SVD reconstruction $H_\alpha[z] = Z_\alpha$ is calculated. The information content of individual single projections Q^S is shown vertically from top to bottom (Figure 4 (c)), for the convenience of comparison with a sinogram. The choice of projections for the subsequent use in the reconstruction is automatically carried out by searching for local maxima, according to the number M of preset informative projections. The reconstruction, or a minimum norm solution Z_α is shown in (Figure 4 (d)), and the difference between the textile image z and its ridge approximation Z_α can be seen in (Figure 4 (e)).

The experiments performed show that the global search (3.2) for M ($M \ll n$) informative directions within total n projections, can be accelerated using the one-dimensional search for M local maxima of the informativity Q^S of individual projections (3.3).

We did not use additional image enhancement tricks in the numerical examples. It should be noted that the additive model used is only an idealized assumption and in the future research has to be added by a nonlinear distortion inclusion (or implantation of anomalies) model.

7 Conclusion

The singular value decomposition algorithm for the Radon transform has shown a sufficiently accurate reconstruction of smooth approximations of regular textures. We have performed computational experiments to illustrate the efficiency of the ridge functions as applied to the method of interpolating the damaged parts of an image and to repair its surrounding areas. We consider the task of inpainting in terms of the Radon integral transform, where the ridge functions allow the use of anisotropy information in the analysis of regular textures in the explicit form. The experimental results in the visual inspection of structural textures, show a certain benefit in decomposition of a texture into a sum of a few ridge functions.

Funding: This work was partially supported by the state contract with the Institute of Computational Mathematics and Mathematical Geophysics (project no. 0251-2021-0003) and by the Ministry of Science of the Republic Kazakhstan (project no. AP09258836).

References

[1] M. Bertalmio, L. Vese, G. Sapiro and S. Osher, Simultaneous structure and texture image inpainting, *IEEE Trans. Image Process.* **12** (2003), 882–889.

[2] P. Brodatz, *Textures: A Photographic Album for Artists and Designers*, Dover, New York, 1966.

[3] K. Hanbay, M. F. Talu and Ö. F. Özgüven, Fabric defect detection systems and methods A systematic literature review, *Optik* **127** (2016), 11960–11973.

[4] R. M. Haralick, Statistical and structural approaches to textures, *Proc. IEEE* **67** (1979), 786–804.
[5] V. E. Ismailov, Notes on ridge functions and neural networks, preprint (2020), https://arxiv.org/abs/2005.14125.
[6] I. G. Kazantsev, Tomographic reconstruction from arbitrary directions using ridge functions, *Inverse Problems* **14** (1998), 635–645.
[7] I. G. Kazantsev and I. Lemahieu, Reconstruction of elongated structures using ridge functions and natural pixels, *Inverse Problems* **16** (2000), 505–517.
[8] Á. G. Legaz-Aparicio, R. Verdú-Monedero and K. Engan, Noise robust and rotation invariant framework for texture analysis and classification, *Appl. Math. Comput.* **335** (2018), 124–132.
[9] F. Li and X. Lv, A Decoupled method for image inpainting with patch-based low rank regulariztion, *Appl. Math. Comput.* **314** (2017), 334–348.
[10] B. F. Logan and L. A. Shepp, Optimal reconstruction of a function from its projections, *Duke Math. J.* **42** (1975), 645–659.
[11] P. M. Mahajan, S. R. Kolhe and P. M. Patil, A review of automatic fabric defect detection techniques, *Adv. Comput. Math.* **1** (2009), 18–29.
[12] P. Maurel, J. F. Aujol and G. Peyré, Locally parallel textures modelling, *SIAM J. Imaging Sci.* **4** (2011), 413–447. .
[13] F. Natterer, *The Mathematics of Computerized Tomography*, Teubner and Wiley, New York, 1986.
[14] H. Y. T. Ngan, G. K. H. Pang and N. H. C. Yung, Automated fabric defect detection a review, *Image Vis. Comput.* **29** (2011), 442–458.
[15] M. Petrou and S. Kamata, *Image Processing Dealing with Texture*, 2nd ed., Wiley, New York, 2021.
[16] A. Pinkus, *Ridge Functions*, Cambridge University, Cambridge, 2015.
[17] C. Schönlieb, *Partial Differential Equation Methods for Image Inpainting*, Cambridge University, Cambridge, 2016.
[18] M. Tuceryan and A. Jain, Texture analysis, in: *The Handbook of Pattern Recognition and Computer Vision*, World Scientific, River Edge (1998), 207–248.
[19] L. A. Vese and S. J. Osher, Modeling textures with total variation minimization and oscillating patterns in image processing, *J. Sci. Comput.* **19** (2003), 553–572.
[20] W. K. Wong, *Applications of Computer Vision in Fashion and Textiles*, Woodhead, Sawston, 2018.
[21] Defect Inspection GLSR Dataset. URL: https://github.com/jjcao/Fabric-Defect-Inspection-GLSR.